Catalytic and Biophysical Properties of a Nitrogenase Apo-MoFe Protein Produced by a *nifB*-Deletion Mutant of *Azotobacter vinelandii*†

Jason Christiansen,‡ Paul J. Goodwin,‡ William N. Lanzilotta,§ Lance C. Seefeldt,*,§ and Dennis R. Dean*,‡

Department of Biochemistry, Fralin Biotechnology Center, Virginia Tech, Blacksburg, Virginia 24061, and Department of Chemistry and Biochemistry, Utah State University, Logan, Utah 84322

Received May 18, 1998; Revised Manuscript Received July 10, 1998

ABSTRACT: A Zn-immobilized metal-affinity chromatography technique was used to purify a poly-histidine-tagged, FeMo-cofactorless MoFe protein (apo-MoFe protein) from a *nifB*-deletion mutant of *Azotobacter vinelandii*. Apo-MoFe protein prepared in this way was obtained in sufficient concentrations for detailed catalytic, kinetic, and spectroscopic analyses. Metal analysis and electron paramagnetic resonance spectroscopy (EPR) were used to show that the apo-MoFe protein does not contain FeMo-cofactor. The EPR of the as-isolated apo-MoFe protein is featureless except for a minor $S = {}^1/_2$ signal probably arising from the presence of either a damaged P cluster or a P cluster precursor. The apo-MoFe protein has an $\alpha_2\beta_2$ subunit composition and can be activated to 80% of the theoretical MoFe protein value by the addition of isolated FeMo-cofactor. Oxidation of the as-isolated apo-MoFe protein by indigodisulfonate was used to elicit the parallel mode EPR signal indicative of the two-electron oxidized form of the P cluster (P^{2+}). The midpoint potential of the P^N/P^{2+} redox couple for the apo-MoFe protein was shown to be shifted by −63 mV when compared to the same redox couple for the intact MoFe protein. Although the apo-MoFe protein is not able to catalyze the reduction of substrates under turnover conditions, it does support the hydrolysis of MgATP at 60% of the rate supported by the MoFe protein when incubated in the presence of Fe protein. The ability of the apo-MoFe protein to specifically interact with the Fe protein was also shown by stopped-flow techniques and by formation of an apo-MoFe protein−Fe protein complex. Finally, the two-electron oxidized form of the apo-MoFe protein could be reduced to the one-electron oxidized form (P^{1+}) in a reaction that required Fe protein and MgATP. These results are interpreted to indicate that the apo-MoFe protein produced in a *nifB*-deficient genetic backround contains intact P clusters and P cluster polypeptide environments. Small changes in the electronic properties of P clusters contained within the apo-MoFe protein are most likely caused by slight perturbations in their polypeptide environments.

Nitrogenase catalyzes biological nitrogen fixation and is a complex, two-component metalloprotein composed of the iron (Fe) protein and the molybdenum−iron (MoFe) protein (*2*). The Fe protein is a 64 kD homodimer that contains two MgATP binding sites and a single [4Fe-4S] cluster (*3*). The MoFe protein is a 240 kD $\alpha_2\beta_2$ tetramer that contains two pairs of novel metalloclusters, called P clusters and FeMo-cofactors (*4, 5*). The structures of the two nitrogenase component proteins, together with models of their associated metalloclusters, have been determined by X-ray crystallography (*3, 4, 6*). During catalysis the Fe protein serves as a specific reductant of the MoFe protein, which in turn provides the site of substrate reduction (*7*). The most probable direction of electron flow in this process is shown in Scheme 1.

Scheme 1

Fe protein [4Fe-4S] cluster → MoFe protein [P cluster] → MoFe protein [FeMo-cofactor] → substrate

A major challenge of nitrogen fixation research is to understand how the mutliple electrons required for substrate reduction are delivered by the Fe protein and accumulated within the MoFe protein. How P clusters might accept electrons from the Fe protein during intercomponent electron transfer is currently enigmatic because they are believed to be already fully reduced in the as-isolated resting state (*8*). Two approaches that should be useful to probe the function of the P cluster include substitution of amino acids that provide the coordination shell that surrounds the P cluster, and alteration of P cluster function by treatment with small molecule inhibitors of nitrogenase catalysis, such as NO, CN^-, and CO. In the case of nitrogenase there are several caveats to these approaches that, so far, have denied an unambiguous assignment of the role of P clusters in the nitrogenase catalytic mechanism. First, it is not possible to treat the P clusters with small molecule inhibitors of

† Research supported by National Science Foundation Grants MCB-9630127 (to D.R.D.) and MCB-9722937 (to L.C.S.) and USDA postdoctoral fellowship USDA-9603167 (to J.C.).

* To whom correspondence should be addressed. D.R.D.: phone, (540) 231-5895; Fax, (540) 231-7126; e-mail, deandr@vt.edu. L.C.S.: phone, (435) 797-3964; Fax, (435) 797-3390; e-mail, seefeldt@cc.usu.edu.

‡ Virginia Tech.

§ Utah State University.

S0006-2960(98)01165-9 CCC: $15.00
Published on Web 08/18/1998

Table 1: Strains Used in This Study

strain	features
DJ	wild-type *A. vinelandii* parental strain
DJ995	produces MoFe protein that contains seven tandem histidines within the C-terminal region of the α-subunit
DJ1141	produces MoFe protein that contains eight tandem histidines within the N-terminal region of the α-subunit
DJ1003	same as DJ995 but also contains an insertion and deletion mutation within *nifB*
DJ1143	same as DJ1141 but also contains an insertion and deletion mutation within *nifB*

nitrogenase catalysis without also affecting the function of FeMo-cofactor. For this same reason, evaluation of perturbations in the P cluster environment caused by amino acid substitutions cannot be made with complete confidence that new spectroscopic or catalytic features have not been elicited by an attendant alteration in FeMo-cofactor or its polypeptide environment. Finally, we have found that many of the potentially most interesting MoFe proteins altered by site-directed mutagenesis cannot be characterized owing to their lability during the standard purification procedure, which involves a heat step and strong ion-exchange chromatography (*9, 10*).

One possible way to circumvent these problems would be to isolate an FeMo-cofactorless form of the MoFe protein that contains intact P clusters and can be activated by the simple addition of isolated FeMo-cofactor. To be useful for the approaches described above, it is necessary that such a protein be amenable to isolation in sufficient quantities for detailed catalytic, kinetic, and spectroscopic analyses. In the present work, site-directed mutagenesis and gene-replacement techniques were used to construct MoFe proteins that respectively contain poly-histidine sequences near the N- or C-terminus regions of their α-subunits. An immobilized metal-affinity chromatography (IMAC) based technique was developed for the rapid and gentle purification of these MoFe proteins. Gene-directed mutagenesis was also used to construct derivatives of these strains which are inactivated for *nifB* gene function. It has previously been shown that MoFe protein from *nifB*-deficient mutants does not contain FeMo-cofactor but does contain other metal clusters, presumably P clusters (*11, 12*). The same IMAC-based method described above was also used to purify "apo-MoFe protein"[2] from these *nifB*-deficient strains. The catalytic and biophysical properties of the MoFe proteins produced in the present work are described.

EXPERIMENTAL PROCEDURES

Strain Constructions and DNA Biochemistry. Five different *Azotobacter vinelandii* strains were used in the present work (Table 1). These include the following: (i) the high-frequency transforming *A. vinelandii* wild-type strain designated DJ (the strain from which all other mutants were ultimately derived); (ii) a strain that has eight histidine codons placed between the third and fourth codons of the *A. vinelandii* wild-type *nifD* gene (DJ1141) (The *nifD* gene encodes the MoFe protein α-subunit (*13*).) (iii) a strain derived from DJ1141 that also contains an insertion and deletion mutation within the *nifB* gene (DJ1143); (iv) a strain that has seven histidine codons placed between codons 481 and 482 of the wild-type *nifD* gene (DJ995); and (v) a strain derived from DJ995 that also contains an insertion and deletion mutation within the *nifB* gene (DJ1003).

The plasmid used for initiating construction of DJ1141 was designated pDB280. This plasmid contains a 1.1 kb *Kpn*I restriction enzyme fragment that includes portions of the *A. vinelandii nifH* and *nifD* genes (*13*) cloned into the pUC19 vector (*14*). Plasmid pDB280 DNA was digested with *Age*I, and a DNA cartridge encoding eight histidine codons was inserted into this site to form pDB944. The unique *Age*I restriction enzyme site within pDB280 spans the third and fourth codons of *nifD*. The synthetic DNA fragments used to form the cartridge that was inserted into pDB280 to construct pDB944 have the following sequences: 5′CGGTCATCACCATCACCACCATCACCACT3′ and 5′CCGGAGTGGTGATGGTGGTGATGGTGATGA3′. The gene cartridge contained within the *nifD* coding region of pDB944 was then transferred to the *A. vinelandii* chromosome by double-reciprocal recombination events that occurred during transformation using pDB944 as the donor DNA. Procedures for transformation (*15*) and gene replacement (*16, 17*) were performed as previously described. Strain DJ1143 was constructed by transformation of DJ1141 to Km^{R} [1] using pDB218 as the donor DNA. Plasmid pDB218 contains a portion of the *A. vinelandii nifB* gene cloned into the pUC7 vector. Plasmid pDB218 also has an internal portion of the *nifB* gene sequence deleted and replaced by a Km^{R} gene cartridge. The portion of the *nifB* gene deleted in pDB218 is flanked by *Sph*I restriction enzyme sites (*18*). The plasmid used for initiating construction of strain DJ995 was designated pDB875. It contains a 2.9 kb *Sal*I restriction enzyme fragment that includes all of *nifD*, as well as portions of the flanking *nifH* and *nifK* genes (*13*), cloned into the pUC119 cloning vector (*19*). Plasmid pDB875 was digested with *Hin*dIII, and a DNA cartridge encoding seven histidine codons was inserted into this site to form pDB827. The unique *Hin*dIII site within pDB875 spans *nifD* codons 481 and 482. The synthetic DNA fragments used to form the cartridge had the following sequences: 5′AGCTCACCACCATCACCACCACCATGC3′ and 5′AGCTGCATGGTGGTGGTGATGGTGGTG3′. The gene cartridge contained within the *nifD* coding region of pDB827 was then transferred to the *A. vinelandii* chromosome by double-reciprocal recombination events that occurred during transformation using pDB827 as the donor DNA. Strain DJ1003 was constructed by transforming DJ995 to Km^{R} using pDB218 as the donor DNA.

[1] Abbreviations: Km^{R}, kanamycin resistance; EPR, electron paramagnetic resonance; IDS, indigosulfonic acid, indigo disulfonate, indigo carmine; PMSF, phenylmethyl sulfonyl fluoride; I-AEDANS, *N*-iodoacetyl-*N*′-(5 sulfo-1-naphthyl)ethylenediamine; DTT, dithiothreitol; PAGE, polyacrylamide gel electrophoresis; SDS, sodium dodecyl sulfate; IMAC, immobilized metal-affinity chromatography; P^{N}, P cluster in the as-isolated all-ferrous state; P^{1+}, P cluster that is oxidized by one electron relative to the P^{N} state; P^{2+}, P cluster that is oxidized by two electrons relative to the P^{N} state.

[2] The term "apo-MoFe protein" has historically been used to designate MoFe proteins produced by *nifE*, *nifN*, *nifB*, or *nifH* mutants that do not contain FeMo-cofactor. However, the term "apo" is a misnomer because these proteins still retain some form of the P cluster. It has been previously shown that the properties of apo-MoFe proteins produced by *nifE*, *nifN*, or *nifB* mutants are not the same as the properties of the proteins produced by a *nifH* mutant (*1*). In the present work, apo-MoFe protein refers to the form produced by a *nifB*-deficient strain, unless otherwise designated.

Cell Growth and Protein Purification. *A. vinelandii* cells were grown at 30 °C in a 150-L custom-built fermenter (W. B. Moore, Inc. Easton, PA) in modified Burk medium (*20*) containing 10 μM Na_2MoO_4 and 10 mM urea as a nitrogen source. Cultures were sparged with pressurized air (80 L/min at 5 psi) and agitated at 125 rpm. When the cell density reached ≈220 Klett units (red filter), cells were de-repressed for *nif* gene expression by concentration (6-fold) using a custom-built AG Technologies (Needham, MA) tangential-flow concentrator and resuspension in Burk medium with no added nitrogen source (*21*). Harvested cells were stored at −80 °C until used. All protein manipulations were performed under anaerobic conditions maintained using either a Schlenk apparatus (*9*) or an anaerobic glovebox.

Crude extracts were prepared by the osmotic shock method (*22*) in a degassed buffer that contained 25 mM Tris−HCl (pH 7.9) and 1 mM sodium dithionite. For crude extract preparation, the buffer also contained 0.2 mM PMSF to inhibit protease activity. Prior to purification, the extracts were brought to 500 mM in NaCl by the addition of degassed, granular NaCl. Approximately 360 g of cells (wet weight) was processed for each purification. Poly-histidine-tagged proteins were purified using immobilized metal-affinity chromatography (IMAC) and DEAE−Sepharose anion-exchange chromatography (Amersham-Pharmacia, Piscataway, NJ). Column eluents were monitored at A_{405} using a Pharmacia UV-1 optical detector and control unit (Amersham-Pharmacia, Piscataway, NJ).

Cell extracts were loaded onto a Zn(II)-charged IMAC column (90 mL of resin in a 2.5 cm × 30 cm column) using a peristaltic pump. After loading the extract, the column was washed with three column volumes of Buffer A (25 mM Tris−HCl, pH 7.9, 500 mM NaCl, 1 mM sodium dithionite) containing 40 mM imidazole−HCl. The protein that remained bound to the column was then eluted using Buffer A containing 250 mM imidazole−HCl. The eluted protein was collected and diluted 8-fold in a degassed buffer (25 mM Tris−HCl, pH 8.0) containing 1 mM sodium dithionite. The diluted protein was then loaded onto a DEAE−Sepharose column (30 mL of resin in a 1.5 cm × 15 cm column) and eluted using a linear NaCl gradient (100−300 mM NaCl over 5 column volumes). Proteins eluted and were collected at approximately 250 mM NaCl. Proteins were concentrated using an Amicon concentrator (Beverly, MA) fitted with a YM100 filter. Protein was quantitated by a modified biuret method using bovine serum albumin as the standard (*23*), and protein purity was monitored by SDS−PAGE electrophoresis (*24*). The final purified product was pelleted and stored in liquid nitrogen until used.

The Fe protein used in all experiments did not possess a poly-histidine tag and was purified from wild-type *A. vinelandii* cells using standard methods (*9*, *25*). The Fe protein used in these studies was found to be electrophoretically pure as demonstrated by a single band migrating on SDS−PAGE gels (*24*).

Assays. Nitrogenase assays were performed as previously described (*10*, *25*). FeMo-cofactor was extracted into NMF and concentrated as previously described (*26*). For apo-MoFe protein activation experiments, 5 μL of isolated FeMo-cofactor (0.31 mg/L in Fe, 0.05 mg/L in Mo) was added to 50 μg of purified apo-MoFe protein and allowed to incubate for 5 min with gentle shaking in a 30 °C water bath. MoFe protein control samples followed the same steps with or without the addition of isolated FeMo-cofactor. FeMo-cofactor-treated protein was then assayed by the addition of 450 μg of purified Fe protein. The samples were incubated for 8 min with gentle shaking in a 30 °C water bath, and the reaction was terminated by addition of 250 μL of a 0.4 M EDTA solution. H_2 production was monitored by injection of 200 μL of the gas phase into a Shimadzu (Kyoto, Japan) GC-14 equipped with a Supelco 80/100 molecular sieve 5A column and a TCD detector. Acetylene reduction assays were performed under a 10% acetylene atmosphere and monitored using a Hewlett-Packard (Avondale, PA) 5890A gas chromatograph equipped with an Al_2O_3 capillary column and a FID detector.

MgATP hydrolysis was determined by a colorimetric assay (*27*) that measures the rate of creatine produced from the MgATP regenerating system used in the activity assay samples described above.

Metal Analysis. Fe was quantitated by the α,α′ bipyridyl method (*28*), and Mo was quantitated by inductively coupled plasma emission (Utah State University, Soil Testing Laboratory).

Chemical Modification of Cysteines. The alkylating reagent, I-AEDANS, was used to determine if the apo-MoFe protein has solvent-exposed sulfhydryl groups. For this analysis 130 μg of protein was brought up to a volume of 40 μL by the addition of 0.5 M Tris−HCl, pH 8.0, 1 mM sodium dithionite. The alkylation reaction was initiated by addition of 10 μL of a 10 mM I-AEDANS solution to the protein sample followed by incubation at room temperature. The alkylation reaction was terminated at specific time points by the addition of 10 μL of a 1.0 M DTT solution to the sample. Approximately 10 μg of I-AEDANS-treated protein was then loaded onto an SDS−PAGE gel (*24*) to separate the individual protein bands and to remove excess I-AEDANS. Protein alkylation was visualized by UV illumination of the PAGE gel prior to staining with Coomassie brilliant blue.

UV/Vis Absorption Spectroscopy. UV/Vis spectra were collected on a Hewlett-Packard 8452A diode array spectrophotometer. The samples were prepared by passage over a Sephadex G-25 column to remove sodium dithionite or a Dowex 1X8-100 ion-exchange column (Sigma, St. Louis, MO) to remove IDS. The samples were sealed inside a 1 cm path length quartz cuvette under anoxic conditions (*29*). The final protein concentration was 1.2 mg/mL for all samples.

EPR and Redox Titrations of MoFe Protein and Apo-MoFe Protein. EPR spectra were recorded on a Bruker (Freemont, CA) ESP300E spectrometer equipped with a dual mode cavity and an Oxford (Concord, MA) ESR 900 liquid helium cryostat. Unless otherwise noted, all spectra were recorded as follows: Parallel mode spectra were recorded at 12 K with a microwave power of 10.1 mW, a microwave frequency of 9.39 GHz, a modulation amplitude of 8.0 G, a modulation frequency of 100 kHz, and a time constant and a conversion time of 10.24 ms each. In each case, the final spectrum was the sum of 20 scans. EPR spectra acquired in perpendicular mode were recorded at 12 K with a microwave power of 6.36 mW, a microwave frequency of 9.64 GHz, a modulation amplitude of 8.0 G, a modulation frequency of 100 kHz, and a time constant and a conversion

time of 10.24 ms. For each case, the final spectrum was the sum of 10 scans.

Potentiometric redox titrations were performed essentially as previously described (*30*). Protein samples were prepared for redox titrations by first passing them over a Sephadex G-25 column equilibrated with the appropriate buffer and at the required pH value. For all redox titrations, the redox mediators flavin mononucleotide ($E_m = -172$ and -238 mV), benzyl viologen ($E_m = -361$ mV), and methyl viologen ($E_m = -440$ mV) were used at final concentrations of 50 μM each. The redox potential of the titration solution was adjusted by the addition of small aliquots of a 2 mM sodium dithionite solution or an oxidized 25 mM IDS solution. At defined potentials, 250 μL aliquots were removed from the titration solution and were immediately frozen in calibrated quartz EPR tubes (Wilmad Co., Buena, NJ). The final concentration for each protein sample analyzed was approximately 75 μM. The reference electrode was a Ag/AgCl microelectrode calibrated against a standard calomel electrode. The electrode calibration was confirmed by performing a redox titration of MoFe protein at pH 8.0, which has a known $E_m = -309$ mV (vs NHE) (*31*). All potentials are reported relative to the normal hydrogen electrode (NHE).

For analysis of the titration data, the relative concentration of the P^{2+} state of the P cluster was quantified from the peak-to-baseline height of the $S \geq 3$ parallel mode EPR signal at $g = 11.8$ (*8*, *31*, *32*). Normalized signal intensities were determined by comparing each signal intensity to the maximum intensity observed at positive potentials. The relative signal intensities were plotted against the applied potential, and each data set was fit to the Nernst equation for a one-electron transfer (*33*).

Activation of Apo-MoFe Protein as Monitored by EPR. The same apo-MoFe protein−FeMo-cofactor ratio used in the activation assays described above (50 μg:5 μL) was used to examine the EPR of apo-MoFe protein activated by FeMo-cofactor. A 250 μL sample of 36.5 mg/mL apo-MoFe protein was diluted into 183 mL of 25 mM HEPES, pH 7.4, and 1 mM sodium dithionite. Isolated FeMo-cofoactor (total volume 1.8 mL) was then slowly added to the solution with gentle mixing. After a 5 min incubation at 30 °C, the mixture was loaded onto a DEAE Sepharose column (10 mL resin, 0.5 × 20 cm column) equilibrated in 25 mM Tris−HCl, pH 8.0, and 1 mM sodium dithionite. Excess FeMo-cofactor was removed by washing the column with 3 volumes of 100 mM NaCl, 25 mM Tris−HCl, pH 8.0, and 1 mM sodium dithionite. FeMo-cofactor-treated MoFe protein was then eluted using a linear salt gradient of 100−300 mM NaCl over 4 column volumes. A 250 μL sample of the reconstituted protein (6 mg/mL) was loaded under anoxic conditions into a quartz EPR tube, and the EPR spectrum was recorded as described above.

Stopped-Flow Spectrophotometry. The apparent rate constant for the dissociation of the Fe protein−MoFe protein complex was determined from stopped-flow experiments by measuring the decrease in A_{430} during the transition of Fe protein from an oxidized to a reduced state as it dissociates from the MoFe protein and is reduced by sodium dithionite (*34*). Rate constants were determined by fitting the data to a single-exponential function. For these experiments, sodium dithionite was removed from the reduced, as-isolated, proteins and exchanged into a 50 mM HEPES buffer, pH 7.4, by passage over a Sephadex G-25 column. Oxidized Fe protein was generated by treating the as-isolated Fe protein with increments of a 25 mM IDS solution until a persistent blue color was observed. IDS was then removed by passing the sample over a Dowex anion-exchange column. Experiments were performed using a Hi-Tech SF61 stopped-flow spectrophotometer, equipped with a computer-controlled data acquisition and analysis package (Hi-Tech, Salisbury, Wilts, UK). The SHU-61 sample handling/mixing unit was kept inside an anaerobic glovebox, and temperature was maintained at 22.4 ± 0.1 °C with a Techne C-85D closed cycle water circulator attached to a Techne FC-200 flow cooler (Techne Ltd., Duxford, Cambridge, U.K.). For each experiment, syringe A contained 40 μM IDS-oxidized Fe protein, 40 μM MoFe protein, 5 mM MgADP, and 200 mM NaCl in a 50 mM HEPES buffer, pH 7.4, and syringe B contained 200 μM reduced Fe protein, and 10 mM Na dithioninte in 50 mM HEPES buffer, pH 7.4. For those experiments involving apo-MoFe protein, identical experimental conditions were used except that MoFe protein was replaced with apo-MoFe protein.

The rate constant for primary electron transfer from the reduced Fe protein to the MoFe protein was also determined using stopped-flow and was monitored by an increase in A_{430} that occurs as the Fe protein becomes oxidized during turnover. For these conditions, the apparent first-order rate constant of primary electron transfer can be determined by fitting the data to a single-exponential function (*35*, *36*). In these experiments syringe A contained 20 μM MoFe protein, 10 mM MgATP, and 10 mM sodium dithionite in 50 mM HEPES buffer, pH 7.4, and syringe B contained 80 μM Fe protein and 10 mM sodium dithionite in 50 mM HEPES buffer, pH 7.4.

Complex Formation. Two different methods were used to assess complex formation between the Fe protein and different forms of the MoFe protein. One method involved the use of an altered Fe protein that is deleted for residue Leu^{127} (ΔL127 Fe protein) (*37*). The second method involved the use of a phosphate analogue, AlF_4^-, and MgATP to capture the Fe protein−MoFe protein complex (*38*, *39*). In both types of experiments, a Superose-12 gel exclusion column (Pharmacia, Piscataway, NJ) equilibrated in 100 mM MOPS buffer, 25 mM Tris, pH 7.3, 100 mM NaCl, and 2 mM sodium dithionite was used for chromatography. The column eluent was monitored using a Pharmacia UV-1 detector and control unit (see above). Fe protein and MoFe protein were added in a 4:1 molar ratio for both types of experiments.

Electron Transfer to the Apo-MoFe Protein. To determine if the Fe protein is able to transfer electrons to the oxidized P clusters of the apo-MoFe protein, EPR spectroscopy was used to monitor the signals from the nitrogenase metal clusters. For these experiments all proteins were exchanged into a 50 mM MOPS buffer, pH 7.0, that contained 2 mM sodium dithionite. MoFe and apo-MoFe proteins were first oxidized with IDS which was then removed by passing the sample over a Dowex anion-exchange column. Sodium dithionite was removed from the Fe protein by passage over a Sephadex G-25 column. Proteins were prepared in an Fe

protein−MoFe protein ratio of 2:1 in the presence of either 2.5 mM MgATP or MgADP. Samples of the individual MoFe/apo-MoFe proteins, together with Fe protein and the appropriate nucleotide, were flash-frozen in a hexane/liquid nitrogen slurry and monitored by EPR. For parallel mode EPR, each plot shown is the sum of 40 scans collected at 17 K with a microwave frequency of 9.4 GHz, a microwave power of 20.1 mW, a modulation amplitude of 12.6 G at a frequency of 100 kHz, and a conversion time and a time constant of 20.48 ms. For perpendicular mode EPR, the spectra are the sum of 50 scans collected at 17 K with a microwave frequency of 9.64 Ghz, a microwave power of 10.1 mW, a modulation amplitude of 8.0 G at a frequency of 100 kHz, and a conversion time and a time constant of 20.48 ms.

RESULTS

Purification and Characterization of Poly-Histidine-Tagged MoFe Proteins. Two mutant strains were constructed for which IMAC-based methods could be applied to MoFe protein purification (Table 1). One of these mutants (DJ1141) has eight histidine codons inserted between the third and fourth codons of the *nifD* gene and produces a modified MoFe protein that has a histidine tag located near the N-terminus of each of its α-subunits. The other strain (DJ995) has seven histidine codons inserted between *nifD* codons 481 and 482 and produces a modified MoFe protein having a histidine tag located near the C-terminus of each of its α-subunits. A third strain was constructed that produces a modified MoFe protein containing the same poly-histidine stretch within the C-terminal region of the MoFe protein α-subunits as DJ995, but it also contains a factor Xa cleavage site (Ile-Glu-Gly-Arg) preceding the poly-histidine-tagged sequences. However, MoFe protein produced by this strain could not be cleaved by treatment with factor Xa protease under anaerobic conditions that included the presence of 1.0 mM sodium dithionite in the buffer, so it was not studied further.

MoFe proteins that contained poly-histidine tags at either the N-terminal or C-terminal regions of their respective α-subunits were isolated from crude extracts of nitrogenase-derepressed DJ1141 (N-tag) or DJ995 (C-tag) cells using a simple four-step procedure that includes the following: (i) passing approximately 30 g of crude extract protein over a Zn(II)-charged IMAC column, (ii) washing the column with Buffer A containing 40 mM imidazole, (iii) eluting the bound protein with Buffer A containing 250 mM imidazole, and (iv) DEAE−Sepharose ion-exchange column chromatography. The entire procedure can be completed in about 12 h and routinely yields approximately 1.2 g of electrophoretically pure MoFe protein for each 30 g of crude extract protein processed. Also, the heme-containing protein that is often found as a persistent contaminant in preparations of MoFe protein when traditional chromatography methods are used (*40*) is not found when MoFe protein is isolated using the IMAC-based method described here.

MoFe protein isolated from extracts of the wild-type DJ strain by using the traditional purification protocol (*9, 10*) was compared to poly-histidine-tagged MoFe proteins purified using the IMAC-based method. These comparisons include the following catalytic, kinetic, and spectroscopic parameters: (i) proton reduction specific activity (2000−2400 nmol of H_2 formed min^{-1} mg of MoFe $protein^{-1}$), (ii) acetylene reduction specific activity (1800−2100 nmol of acetylene reduced min^{-1} mg of MoFe $protein^{-1}$), (iii) rate of MgATP hydrolysis observed in hydrogen- or acetylene-reduction assays (4.5−5.5 MgATP hydrolyzed/each 2 e^- transferred to product), (iv) the amount of Fe protein needed to achieve half the maximum activity (2.5−3.2 μM of Fe protein per approximately 0.42 μM of MoFe protein used in a 1.0 mL assay), (v) rate constant of primary electron transfer from the Fe protein to the MoFe protein (120−160 s^{-1}), (vi) Fe protein−MoFe protein dissociation rate constant (4.4−6.5 s^{-1}), (vii) presence of the characteristic $S = {}^3/_2$ perpendicular mode EPR spectrum indicative of the FeMo-cofactor ($g = 4.3, 3.7, 2.0$, [*41*], see Figure 4), (viii) presence of the characteristic parallel mode EPR spectrum indicative of oxidized P clusters (P^{2+}, $g \approx 11.8$, [*8, 31, 32*], see Figure 5) and, (ix) all three MoFe proteins also exhibited the ability to form a tight complex when incubated with the Fe protein in the presence of MgATP and AlF_4^- or when incubated with ΔL127 Fe protein. There is some variation from certain published values determined by different investigators because most kinetic and catalytic parameters of nitrogenase depend on the protein concentration, the assay pH, the component protein ratios, and the salt concentration (*42−45*). All three MoFe protein types characterized in the present work were examined under identical experimental conditions for each parameter tested. Thus, a lack of a substantial difference for any of the catalytic, kinetic, or spectroscopic features measured for the three forms of MoFe protein characterized here indicates that neither of the poly-histidine-tagged versions of the MoFe protein are appreciably different from the normal MoFe protein in terms of their catalytic or biophysical properties. This conclusion is further supported by the observation that strains DJ, DJ1141 (N-tag), and DJ995 (C-tag) all exhibit the same diazotrophic growth rates. Because strains DJ1141 (N-tag) and DJ995 (C-tag) produce proteins having nearly identical properties, only strain DJ1141 (N-tag), and derivatives thereof, were studied further in the present work.

IMAC Purification of Apo-MoFe Protein. Strain DJ1141 (N-tag) was used as the parental strain to construct a mutant strain deleted for *nifB* (DJ1143). Previous work has shown that MoFe protein produced from this genetic background does not contain FeMo-cofactor, but does contain other metal centers, presumably P clusters (*11, 12, 26*) (MoFe protein that does not contain FeMo-cofactor is referred to as apo-MoFe protein[2]). Hereafter, MoFe protein will refer to the poly-histidine-modified form produced by strain DJ1141 (N-tag), and apo-MoFe protein will refer to the poly-histidine-modified form produced by DJ1143. By using the same IMAC-based approach described above, it was possible to purify approximately 400 mg of apo-MoFe protein/30 g of DJ1143 crude extract protein processed. Figure 1 shows an SDS−PAGE gel for a typical purification of apo-MoFe protein. Metal analyses of purified apo-MoFe proteins yielded ∼13 Fe atoms/tetramer and no detectable molybdenum.

Time-Dependent Alkylation of MoFe Protein and Apo-MoFe Protein. Figure 2 shows a comparison of the time course for alkylation of MoFe protein and apo-MoFe protein. For the apo-MoFe protein, there is already some apparent

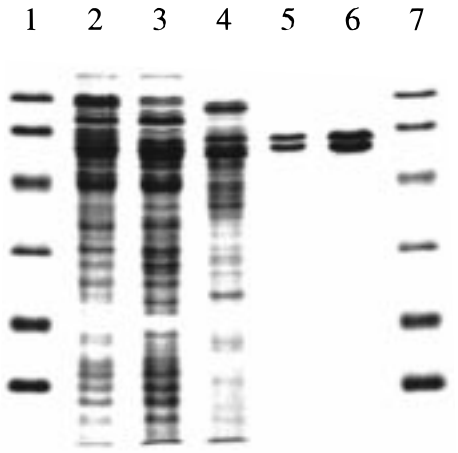

FIGURE 1: SDS−PAGE for the IMAC purification of apo-MoFe protein (DJ1143). Proteins were separated using SDS−PAGE with a 4% stacking gel and a 20% running gel and then stained with Coomassie brilliant blue: lanes 1 and 7, M_r standards, (from top: phosphorylase b, 97 400; serum albumin, 66 200; carbonic anhydrase, 31 000; soybean trypsin inhibitor, 21 500; lysozyme, 14 400); lane 2, sample of crude extract that was loaded onto the IMAC column; lane 3, IMAC column flow through; lane 4, IMAC column eluent from Buffer A, 20 mM imidazole−HCl wash; lane 5, protein collected from the Buffer A, 250 mM imidazole−HCl elution; lane 6, purified apo-MoFe protein from DEAE column fraction. For lane 2 the amount of protein loaded was ~30 μg, and for lane 6 the amount of protein loaded was ~10 μg. For the other lanes the amount of protein loaded was not determined.

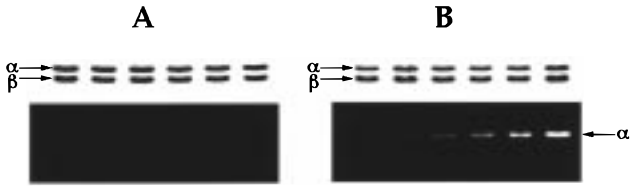

FIGURE 2: Time course for the alkylation of the isolated MoFe protein and apo-MoFe protein. Coomassie-stained SDS−PAGE gels of MoFe protein (panel A, top) and apo-MoFe protein (panel B, top) treated with I-AEDANS as described in the Experimental Section. Each lane was loaded with ~10 μg of I-AEDANS-treated protein. The leftmost lane in both gels is a control, where the MoFe protein or apo-MoFe protein was not treated with I-AEDANS, and the lanes that follow correspond to 1, 5, 10, 15, and 30 s I-AEDANS incubations, respectively. The SDS−PAGE gel of MoFe protein (panel A, bottom) and apo-MoFe protein (panel B, bottom) was visualized with UV light prior to Coomassie staining. The apo-MoFe protein alkylates rapidly, while the MoFe protein is not modified during the same time period. The locations of the α- and β-subunits of the MoFe and apo-MoFe proteins are indicated by arrows for the SDS−PAGE gels in both panels.

alkylation after only 1 s of I-AEDANS treatment (Figure 2, panel B). However, even after a 30 s I-AEDANS treatment, intact MoFe protein does not show any modification (Figure 2, panel A). These results are consistent with those reported by Magnuson, et al. (*46*) who showed that apo-MoFe protein has two cysteines (residues α-Cys-45 and α-Cys-275) that are readily alkylated, whereas the intact MoFe protein is not susceptible to rapid alkylation. In a separate experiment, a 20 min, anoxic incubation of isolated apo-MoFe protein (7.3 μM in 1 mL) with a 1 mM α,α′ bipyridyl solution did not result in a change in the A_{520}. Thus, the iron contained within the intact apo-MoFe protein is not accessible to the metal-chelating reagent α,α′ bipyridyl. However, upon exposing

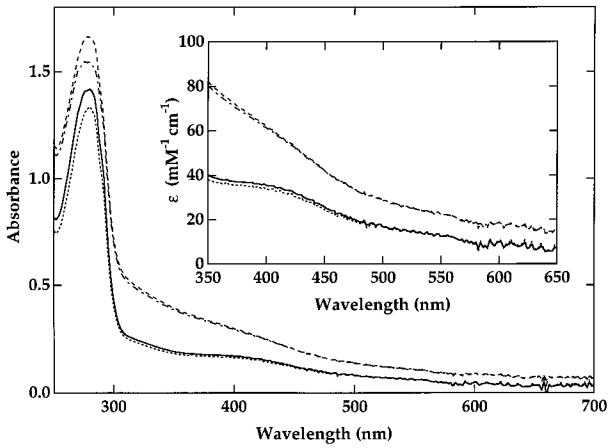

FIGURE 3: UV/vis spectra of the apo-MoFe protein and MoFe protein. Spectra of the as-isolated (solid line) and IDS-oxidized (dotted line) apo-MoFe protein. Also shown is the UV/vis spectrum of the MoFe protein in the as-isolated (dash−dot) and IDS-oxidized (dashed) forms. Before taking the spectra, sodium dithionite or IDS was removed by anaerobic buffer exchange using either a G-25 column or a Dowex strong anion-exchange column, respectively. Protein concentrations were maintained at 1.2 mg/mL for each spectrum. The inset shows the 350−700 nm visible region with the *y*-axis converted to units of absorption coefficient (ϵ).

the same sample to air, the A_{520} showed a 7-fold increase within one minute.

UV/Vis Spectroscopic Properties of Apo-MoFe Protein. Isolated apo-MoFe protein has a distinct maroon color that is readily distinquished from the greenish-brown color of purified MoFe protein. The UV/vis spectra of the reduced, as-isolated, and IDS-oxidized, forms of the MoFe protein and the apo-MoFe protein are shown in Figure 3. The respective spectra of the MoFe protein and the apo-MoFe protein are essentially featureless in the 350−700 nm range. For the apo-MoFe protein, the amplitude in the visible range is lower when compared to that for the MoFe protein. The inset to Figure 3 shows that at 400 nm, the reduced apo-MoFe protein has an $\epsilon_{400} = 35.5$ mM^{-1} cm^{-1}, whereas the reduced MoFe protein has an $\epsilon_{400} = 62.3$ mM^{-1} cm^{-1} (*47*). Another property is that the respective ϵ_{400} values for neither the apo-MoFe protein nor the MoFe protein appreciably change upon their oxidation by IDS (*48*).

Activation of Apo-MoFe Protein. The as-isolated apo-MoFe protein does not exhibit the $S = {}^3/_2$ EPR signal that is characteristic of the MoFe protein or isolated FeMo-cofactor (*41, 49*), a result that is consistent with the expectation that apo-MoFe protein does not contain any FeMo-cofactor (Figure 4A). This result is also consistent with metal analyses that failed to detect any Mo associated with the as-isolated apo-MoFe protein. Although there is no $S = {}^3/_2$ EPR signal present in the as-isolated apo-MoFe protein, there is an $S = {}^1/_2$ signal that is recognized in the $g = 2$ region and that disappears completely above 30 K. Spin quantitation of this species revealed that it is a very minor component representing less than 0.05 spins/apo-MoFe protein.

Apo-MoFe protein could be activated by the addition of isolated FeMo-cofactor to yield a MoFe protein that exhibits an $S = {}^3/_2$ EPR signal that is identical in line shape and *g* values to the isolated MoFe protein (Figure 4B) and does not exhibit the broad spectral features seen in the EPR of isolated FeMo-cofactor (*49*). As discussed below, a small

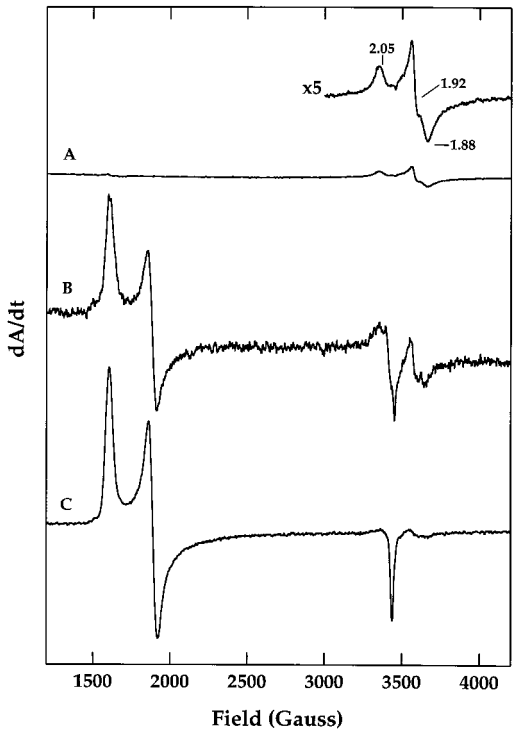

FIGURE 4: Activation of apo-MoFe protein observed using EPR. (A) Perpendicular mode EPR of the apo-MoFe protein (36.5 mg/mL, 10 scans). The inset in the upper right corner is a 5× blow-up of the $g_{av} = 1.95$ signal with the associated g values shown. (B) Perpendicular mode EPR spectrum of the activated apo-MoFe protein (6 mg/mL, 30 scans), activated as described in the text. (C) EPR of MoFe protein (62.7 mg/mL, 10 scans). All spectra have been amplitude corrected for protein concentration (and also for power in the case of the MoFe protein spectrum). Spectra were collected at 12 K and 9.64 GHz with the following parameters: power 6.36 mW (with the exception of the MoFe protein sample, which was at 0.201 mW), receiver gain 1×10^4, modulation frequency 100 kHz, and modulation amplitude 12.6 G.

$S = {}^1/_2$ EPR signal that is present in the as-isolated apo-MoFe protein persists in the FeMo-cofactor-treated sample. The activated protein has a specific activity of 1600 nmol of H_2 formed min^{-1} mg ^{of} apo-MoFe $protein^{-1}$. The apo-MoFe protein did not exhibit any proton- or acetylene-reduction activity prior to FeMo-cofactor addition. MoFe protein isolated from DJ1141 (N-tag) typically has a specific activity of 2000 nmol of H_2 formed min^{-1} mg of MoFe $protein^{-1}$, so the activation achieved by FeMo-cofactor addition represents about 80% of the theoretical activation value. Attempts to enhance the FeMo-cofactor-dependent activation of apo-MoFe protein by the addition of either dithiothreitol or Fe protein, with or without MgATP, were not successful. Similarly, the addition of crude extracts from a Δ*nifHDK* strain also failed to enhance the activation of apo-MoFe protein.

EPR Spectroscopic Properties of Apo-MoFe Protein. Two EPR signals have been reported that represent two different oxidation states of the P cluster. One of these signals arises from the one-electron oxidation of the P cluster (P^{1+} state) and can be recognized by a rhombic signal in perpendicular mode EPR with g values of 2.05, 1.94, and 1.81 (*50*). The other signal arises from the two-electron oxidized form (P^{2+} state) and can be recognized by a $g \approx 11.8$ peak observed in parallel mode EPR (*8, 31, 32*). At pH 8.0, the pH at which all the proteins were purified in the present work, the P^{1+} EPR signal cannot be observed because the P^{2+}/P^N and P^{2+}/P^{1+} redox couples exhibit the same midpoint potentials (−309 mV, [*31*]). The P^{1+} signal was initially observed for a MoFe protein sample prepared in a pH 7.4 buffer (*50*), and recent work has shown that the P^{2+}/P^{1+} redox couple is pH-dependent (*51*). Thus, by exchanging the protein into a pH 7.4 buffer, and poising the sample at a defined potential, both forms of the oxidized P cluster from the MoFe protein can be observed (Figure 5, A and B, trace 2). For similarly treated apo-MoFe protein, both of the P^{1+} and P^{2+} signals, having the same g values and line shapes as those of the corresponding intact MoFe protein signals, can be recognized (Figure 5, A and B, trace 1). The spectra shown in Figure 5B represent the maximum observed intensity of the P^{1+} signal for the samples run. However, each sample had to be poised at a different potential for these spectra (see legend to Figure 5) which suggested that the midpoint potentials for the metal cluster in the apo-MoFe protein may be different from that observed in the MoFe protein. Differences between the spectra shown in Figure 5B are due to the contribution of the $g = 2$ feature from the FeMo-cofactor $S = {}^3/_2$ signal in the MoFe protein sample, and the contribution of a mediator-derived radical signal at $g = 2$ in the apo-MoFe protein sample. As discussed below, the P^N/P^{2+} redox couple for the apo-MoFe protein is shifted −63 mV relative to the intact MoFe protein. Thus, a corresponding mediator-derived radical signal is not recognized for intact MoFe protein because the respective samples were poised at different potentials.

By monitoring the amplitude of the P^{2+} EPR signal at pH 8.0, the midpoint potential for the P^N/P^{2+} redox couple can be measured by performing a mediated redox titration. Figure 6 shows titration data with corresponding fits to the Nernst equation for a single electron transfer. The MoFe protein Nernst fit yields a midpoint potential of −314 mV for the P^N/P^{2+} couple, a value that is consistent with previous reports (*52*). In contrast, the apo-MoFe protein Nernst fit renders a midpoint potential of −377 mV, which represents a −63 mV shift relative to the MoFe protein.

Fe Protein−Apo-MoFe Protein Interactions. Incubation of the MoFe protein with Fe protein, sodium dithionite, and MgATP under an argon atmosphere results in the reduction of protons with approximately 4−5 MgATP hydrolyzed for each H_2 evolved (*44*). The maximum rate for H_2 evolution catalyzed by the isolated MoFe protein produced by strain DJ1141 (N-tag) was approximately 2000 nmol of H_2 formed min^{-1} mg of MoFe $protein^{-1}$ with a corresponding MgATP hydrolysis rate of 9800 nmol of MgATP hydrolyzed min^{-1} mg of MoFe $protein^{-1}$ (4.9 MgATP/$2e^-$). Incubation of apo-MoFe protein under the same catalytic conditions resulted in no H_2 evolution, but MgATP hydrolysis occurred at a rate of 5900 nmol of MgATP hydolyzed min^{-1} mg of apo-MoFe $protein^{-1}$, which is about 60% of that supported by the MoFe protein. No MgATP hydrolysis was catalyzed by the apo-MoFe protein in the absence of the Fe protein.

Another way to examine the interaction of the nitrogenase component proteins is to measure the apparent first-order rate constant of dissociation using stopped-flow spectroscopy. As described in the Experimental Section, the dissociation rate constant of the component proteins can be indirectly measured by determining the rate of sodium dithionite-

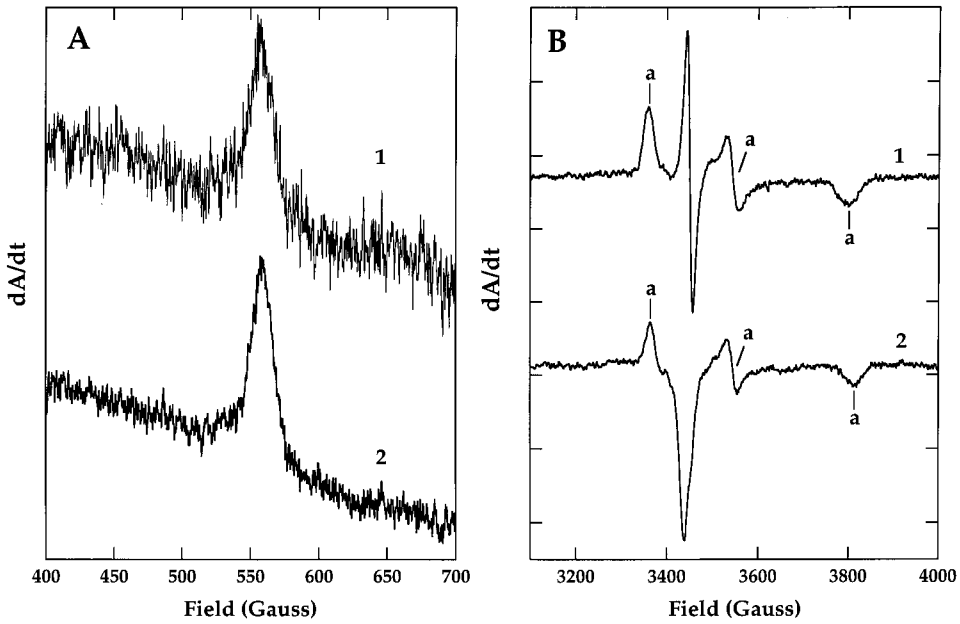

FIGURE 5: EPR spectra of the P^{2+} and P^{1+} states of the P cluster in apo-MoFe and MoFe protein. Representative spectra taken from the redox potential titrations performed as described under experimental methods. (Panel A) Spectra for IDS-oxidized apo-MoFe (trace 1) and IDS-oxidized MoFe proteins (trace 2) in parallel mode at pH 8.0. The MoFe protein P^{2+} signal intensity was adjusted for protein concentration. (Panel B) Spectra for the IDS-oxidized apo-MoFe protein (−306 mV) (trace 1) and MoFe protein (−230 mV) (trace 2) in perpendicular mode at pH 7.4. The P^{1+} signal is indicated by "a" in the figure. The radical signal exhibited in the apo-MoFe protein at ~3450 G arises from the mediator solution (as described in results), while the dip observed for the MoFe protein in the same region is due to the FeMo-cofactor $S = {}^3/_2$ signal.

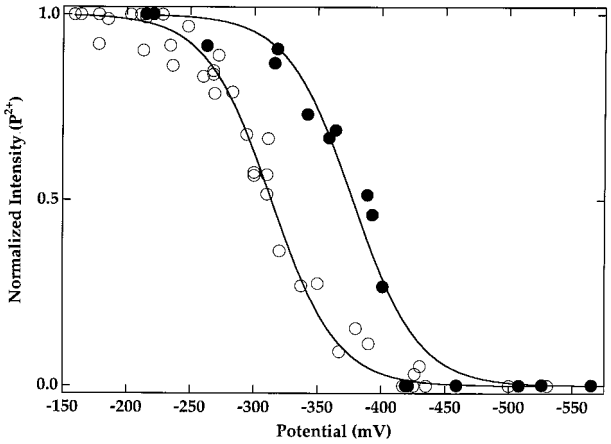

FIGURE 6: Redox titration of the P^{2+} signal from apo-MoFe protein and the MoFe protein. Redox titrations were performed as described in experimental procedures. Normalized intensities of the apo-MoFe protein (●) and the MoFe protein (○) P^{2+} EPR signals are plotted against the applied potential (vs NHE). Data has been fit to the Nernst equation for a one-electron transfer event. Midpoint potentials are −377 and −314 mV for the apo-MoFe protein and the MoFe protein, respectively.

mediated reduction of the oxidized MgADP-bound Fe protein as it is released from the MoFe protein. The measured dissociation rate constant for the MoFe protein−Fe protein−MgADP complex is 3.6 s^{-1}, and the dissociation rate constant for the apo-MoFe protein−Fe protein−MgADP complex is 4.5 s^{-1} (Figure 7). The monophasic behavior of the absorbance decreases observed in Figure 7 indicates that there is only a single active apo-MoFe protein species interacting with the Fe protein. In similar experiments, where the ΔL127 Fe protein is used in place of the Fe protein, the rate of MoFe protein−ΔL127 Fe protein dissociation is too slow to be accurately measured. The dissociation rate constant for the apo-MoFe protein−ΔL127 Fe protein was found to be approximately 1.0 s^{-1}.[3]

Finally, evidence for specific interaction between the apo-MoFe protein and the Fe protein was obtained by complex formation, as evaluated by gel exclusion chromatography, when apo-MoFe protein and Fe protein were incubated in the presence of MgATP and AlF_4^-. These results are similar to those previously reported for the intact MoFe protein (*38*, *39*), except that trapping of all of the available apo-MoFe protein, even when incubated in the presence of a large excess of Fe protein, could not be achieved (data not shown). In contrast, incubation of a molar excess of Fe protein relative to the MoFe protein, together with MgATP and AlF_4^-, resulted in the capture of all the available MoFe protein into a tight complex composed of 2 bound Fe proteins/each MoFe protein tetramer ([*53*], control experiments performed in the present work). Another difference observed between the intact MoFe protein and the apo-MoFe protein was that co-incubation of apo-MoFe protein and Fe protein in the presence of MgATP and AlF_4^- beyond 15 min resulted in precipitation of the sample. All of these results indicate that, although the apo-MoFe protein is able to interact with the Fe protein, this interaction does not appear to be identical to the normal Fe protein−MoFe protein interaction.

Electron Transfer from the Fe Protein to the Apo-MoFe Protein. No apparent primary electron transfer from the reduced Fe protein or ΔL127 Fe protein to the as-isolated apo-MoFe protein could be detected by stopped-flow spectrophotometry. Furthermore, there was neither a loss in the

[3] The value for the dissociation rate constant for the ΔL127 Fe protein from the apo-MoFe protein results from the best fit of a single exponential to the data. For tight protein complexes, the change in absorbance is quite small and difficult to fit accurately, so the value reported here is an approximation.

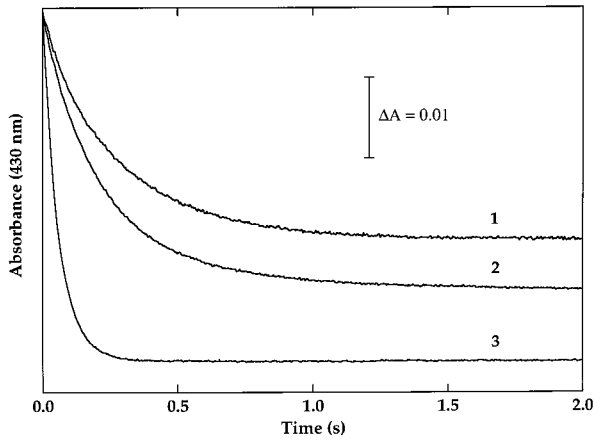

FIGURE 7: Interaction of apo-MoFe protein with Fe protein monitored by stopped-flow spectrophotometry. The interaction of the apo-MoFe and the Fe protein was measured using stopped-flow methods. The apparent first-order rate constant, k, resulted from single-exponential fits to the data. Each trace represents the change in A_{430} that occurred after mixing a solution containing 200 μM Fe protein and 10 mM sodium dithionite in 50 mM HEPES, pH 7.4, with a solution containing the following: (trace 1) 20 μM reduced MoFe protein without sodium dithionite, 20 μM oxidized Fe protein, and 5 mM MgADP, $k = 3.6$ s^{-1}, or (trace 2) 20 μM reduced apo-MoFe protein without sodium dithionite, 20 μM oxidized Fe protein and 5 mM MgADP, $k = 4.5$ s^{-1}. (trace 3) The change in A_{430} that occurred after mixing a 10 mM sodium dithionite solution with a solution containing 20 mM oxidized Fe protein and 5 mM MgADP, $k = 17$ s^{-1}. For all experiments, the oxidized Fe protein syringe contained 50 mM HEPES pH 7.4, 200 mM NaCl for buffer.

$S = {}^1/_2$ EPR signal characteristic of the reduced Fe protein nor the appearance of any new EPR signals when Fe protein and apo-MoFe were co-incubated under turnover conditions. In contrast, MgATP-dependent electron transfer from the Fe protein to apo-MoFe protein in the P^{2+} state was detected. Figure 8 shows the parallel and perpendicular mode EPR spectra of samples where IDS-oxidized apo-MoFe protein (P cluster in the P^{2+} state) and reduced Fe protein were co-incubated in the presence of either MgADP or MgATP. The top spectrum in panel A of Figure 8 shows the presence of the parallel mode P^{2+} EPR signal for the oxidized apo-MoFe protein when incubated with Fe protein and MgADP, indicating that there is no electron transfer under these conditions. However, as shown in the bottom spectrum of panel A, there is no parallel mode P^{2+} EPR signal in a sample for which MgATP was substituted for MgADP, indicating that an electron-transfer event has occurred and the P^{2+} state has been reduced. Panel B shows the spectra of the corresponding samples run in perpendicular mode. In the top trace of panel B the characteristic $S = {}^1/_2$ signature in the $g \approx 2$ region for the reduced Fe protein with MgADP bound (*54*) is evident. In the lower trace, the sample for which MgADP has been replaced by MgATP, the signal in the $g \approx 2$ region observed in the top trace, has disappeared with the attendant appearance of a new signal having g values corresponding to the P^{1+} state of the P cluster. Thus, electron transfer from the reduced Fe protein to the IDS-oxidized apo-MoFe protein occurs only in the presence of MgATP such that the P^{2+} form of the P cluster is reduced to the P^{1+} state. Control experiments using the MoFe protein, rather than the apo-MoFe protein, gave the same results.

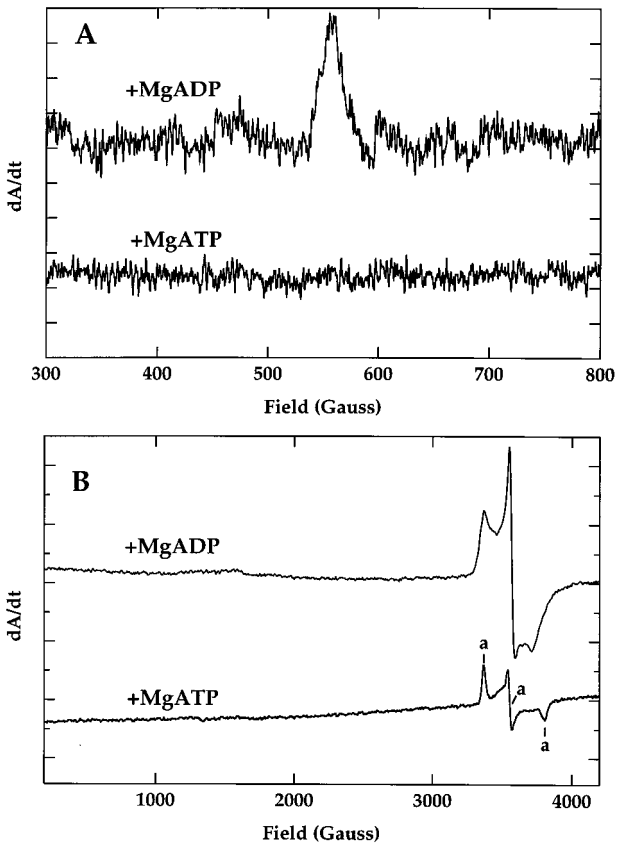

FIGURE 8: MgATP-dependent electron transfer from the Fe protein to the apo-MoFe protein. (Panel A) Parallel mode EPR for IDS-oxidized apo-MoFe protein with reduced, sodium dithionite-free, Fe protein with the addition of MgADP (top) or MgATP (bottom). (Panel B) Perpendicular mode EPR for the same samples in Panel A with the addition of MgADP (top) or MgATP (bottom). As in Figure 5, the $S = {}^1/_2$ portion of the P^{1+} signal is indicated by "a".

DISCUSSION

Two different *A. vinelandii* strains were constructed that produce MoFe proteins having poly-histidine insertions located at, or near, their respective α-subunit C- or N-termini. Both of these modified proteins can be rapidly purified through the application of an IMAC-based procedure and yield proteins having the same catalytic, kinetic, and spectroscopic properties of the normal MoFe protein. Thus, by using the IMAC-based approach, both the heat step and the strong anion-exchange chromatography step, necessary for the traditional purification of MoFe proteins (*9, 10*), can be avoided. By using the appropriately constructed strains and by applying the same IMAC-based purification procedure, it is also possible to purify apo-MoFe protein in concentrations amenable for detailed catalytic and spectroscopic characterizations. Below, the results of the characterization of the apo-MoFe protein isolated in the present work are interpreted and discussed in light of the properties of other apo-MoFe proteins that have been previously described.

Subunit Composition and Activation of Apo-MoFe Protein. Purification of apo-MoFe protein from an *A. vinelandii nifB* mutant has been previously described (*11*). There are two significant differences between the properties of the apo-MoFe protein described here and the one previously characterized. The previously described apo-MoFe protein has

an $\alpha_2\beta_2\gamma_2$ subunit organization and is reported to be 100% activatable by FeMo-cofactor addition (*11*), whereas the apo-MoFe protein described here does not contain the γ-subunit and is activated to 80% of the theoretical value by FeMo-cofactor addition. There is in vitro evidence that γ-stabilizes apo-MoFe protein and that it assists FeMo-cofactor insertion into the apo-MoFe protein (*55*). It is possible that our inability to achieve 100% of the theoretical activation value could be related to the lack of the γ-protein.

There are several possibilities that could explain why there is no γ-protein associated with the apo-MoFe protein described here. One possibility is that the poly-histidine insertion located at the N-terminus of the α-subunit of apo-MoFe protein purified from DJ1143 overlaps the γ-binding site and therefore prevents complex formation between γ and the apo-MoFe protein. This possibility was examined by isolating apo-MoFe protein from DJ1003, which carries a poly-histidine insertion near the C-terminus of the α-subunit. It was determined that this apo-MoFe protein also did not contain the γ-protein. Because the N- and C-termini of the α-subunit of the normal MoFe protein are separated by about 40 Å in the crystallographic model (*56*), it seems unlikely that both C- and N-terminal insertions would eliminate the ability or need for γ to interact with the MoFe protein. Nevertheless, the three-dimensional structure of the apo-MoFe protein is not known, so this remains a reasonable explanation. A second possibility is that the high salt concentration (0.5 M NaCl) present in the early stages of the apo-MoFe protein purification described here, and not present in the previously described purification protocol (*11*), might prevent the interaction of apo-MoFe protein and γ. A final possibility is that γ adventitiously binds to the apo-MoFe protein in the previously described purification procedure. In this context it is noted that expression of γ is not *nif*-regulated nor does it dissociate from the apo-MoFe protein upon activation (*11*). These possibilities will only be resolved once purified γ is available in large quantities and the gene encoding γ can be inactivated in vivo. Whatever the reason for our inability to fully reconstitute the apo-MoFe protein described here, it is clear from the high level of activation that is achieved, and the appearance of a normal $S = {}^3/_2$ EPR signal upon FeMo-cofactor addition, that activation of apo-MoFe protein can be accomplished by the simple addition of isolated FeMo-cofactor and without the presence of the γ-subunit. Also, because the parallel mode P^{2+} EPR signal evoked by IDS oxidation of the apo-MoFe protein shows the same intensity when compared to IDS-oxidized MoFe protein (when adjusted for protein concentration), it is not likely that the apo-MoFe protein we have purified consists of a significant amount of inactivatable species.

There is also an $\alpha_2\beta_2\gamma_2$ subunit organization in the case of apo-MoFe protein produced by *Klebsiella pneumoniae nifB* mutants (*12, 57, 58*). However, in this organism the γ-subunit has been identified as the product of the *nifY* gene, and it does dissociate from the complex upon FeMo-cofactor insertion (*57, 58*), in contrast with the stable hexameric form previously reported for *A. vinelandii* (*11*). There is also a *nifY* gene in *A. vinelandii*, but the function of the *nifY* product in this organism is not yet known, nor is there any phenotype associated with its inactivation (*59*). Even if the *nifY* gene product from *A. vinelandii* is capable of forming a complex with the apo-MoFe protein, it is unlikely that such a complex would be identified in the present work because, on the basis of northern analyses and gene fusion experiments ([*60*], our unpublished work), the expression of *nifY* is much lower than the expression of the genes that encode the MoFe protein subunits. As in the case of the γ protein, the potential involvement of the *A. vinelandii nifY* gene product in FeMo-cofactor insertion or stabilization of the apo-MoFe protein will require the purified protein.

Spectroscopic Features of the Apo-MoFe Protein. The EPR spectrum of the as-isolated apo-MoFe protein is featureless except for a minor $S = {}^1/_2$ signal in the $g \approx 2$ region that has line shape, g values, and temperature dependence very similar to typical [4Fe-4S] clusters (Figure 4, [*61, 62*]). This signal, which integrates to only 0.05 spins/MoFe protein, disappears upon oxidation of the sample and reappears upon re-reduction by sodium dithionite. The signal also persists even after the addition of FeMo-cofactor, although it is somewhat obscured by the contribution of FeMo-cofactor to the EPR spectrum at $g = 2$. Considering the purity of the protein sample, it is unlikely that the observed $S = {}^1/_2$ signal arises from a contaminating protein. A similar $S = {}^1/_2$ EPR signal attributed to a damaged P cluster or a P cluster precursor has been reported previously (*12, 63*). This same signal is also present at 0.1−0.3 spins/mol in an apo-MoFe protein produced by a *nifH*-deletion mutant (*64*). In related work we have purified an apo-MoFe protein form produced by a *nifH*-deletion strain using the IMAC-based approach and confirmed a previous report that it is different from apo-MoFe protein in that it contains a more significant $S = {}^1/_2$ EPR signal (0.5 spins/mol of apo-MoFe protein) and that it cannot be activated by the simple addition of isolated FeMo-cofactor (*1, 64*). We also find that neither the P^{1+} nor P^{2+} EPR signals can be elicited by IDS oxidation of apo-MoFe protein isolated from a *nifH*-deletion strain. On the basis of these observations, we find the proposal that intact P clusters might be formed in a pathway that involves the fusion of two [4Fe-4S] cubanes an attractive one (*63*), and suggest that the species giving rise to the $S = {}^1/_2$ signal from apo-MoFe proteins produced from either *nifH*- or *nifB*-deletion backgrounds represent either incompletely processed or damaged P clusters.

The MoFe protein P clusters have been prepared in five different oxidation states at pH 8.0, as illustrated below ([*52*], Scheme 2). All eight iron atoms present in the P cluster in

Scheme 2

$$P^N \underset{e^-}{\overset{E_{m1} = -309\ mV}{\rightleftharpoons}} P^{1+} \underset{e^-}{\overset{E_{m2} = -309\ mV}{\rightleftharpoons}} P^{2+} \underset{e^-}{\overset{E_{m3} = +90\ mV}{\rightleftharpoons}} P^{3+} \rightarrow P^{superox}$$

the as-isolated MoFe protein are believed to be in the Fe^{2+} oxidation state, and this form of the P cluster is often referred to as P^N (the N designation refers to the native or as-isolated form [*65*]). There is no direct evidence that the P cluster can be reduced to a lower oxidation state. The P^N state of the P cluster can be reversibly oxidized by up to three electron equivalents to respectively yield the oxidation states designated P^{1+}, P^{2+}, and P^{3+} in Scheme 2. The P cluster can be further oxidized beyond the P^{3+} state, but oxidation

to such "superoxidized" states is not reversible (*52*). The P^N state is diamagnetic and therefore EPR silent, whereas both the P^{1+} and P^{2+} states are paramagnetic and have EPR signals. The P^{1+} state has a mixed spin system ($S = {}^1/_2$ and ${}^5/_2$) with perpendicular mode signals in the $g \approx 2$ and 5 regions (*50*). The P^{2+} state has an integer spin system ($S \geq 3$) with a parallel mode EPR signal at $g \approx 11.8$ (*8, 31, 32*). The midpoint potentials for both E_{m1} and E_{m2} (Scheme 2) have been determined to be -309 mV at pH 8.0, and therefore, at pH 8.0 the EPR signal for the P^{1+} oxidation state cannot be observed (*31*). However, the redox couple between P^{1+} and P^{2+} is pH-dependent (*50, 51*), so the P^{1+} state can be readily identified in a sample that has been IDS-oxidized at pH 7.4.

If the apo-MoFe protein has intact P clusters that are structurally and electronically similar to the P clusters present in the MoFe protein, then it should be possible to elicit the P^{1+} and P^{2+} EPR signals by IDS-oxidation of apo-MoFe protein. Panel A in Figure 5 shows the P^{2+} state (parallel mode EPR signal at $g \approx 11.8$) for both the MoFe protein (trace 1) and the apo-MoFe protein (trace 2) by IDS-mediated oxidation at pH 8.0. Panel B in Figure 5 shows the P^{1+} state (perpendicular mode signal in the $g \approx 2$ region) for both the MoFe protein (trace 1) and the apo-MoFe protein (trace 2) by IDS-mediated oxidation at pH 7.4. These observations confirm and extend the work of Robinson et al. (*66*), who concluded from comparative MCD spectroscopy that P clusters present in mature MoFe protein and an apo-MoFe protein produced from a *K. pneumoniae nifB* mutant are electronically very similar or identical to each other (*66*). Nevertheless, comparisons between the present work and that involving the corresponding *K. pneumoniae* proteins must be considered in light of differences between the respective apo-MoFe proteins. For example, the apo-MoFe protein isolated from *K. pneumoniae* contained molybdenum, had an associated γ-subunit, and could only be activated to a very low level.

In the present work it is shown that the respective midpoint potentials for the P^N/P^{2+} redox couple for MoFe protein and apo-MoFe protein are significantly different (-314 vs -377 mV, see Figure 6). Thus, there is a detectable difference in the electronic properties of P clusters from the apo-MoFe protein versus the MoFe protein. It is likely that such differences are the result of modest structural changes in the P cluster polypeptide environment rather than an alternate form of the P cluster. Other evidence that there are some differences in the global structure of apo-MoFe protein when compared to MoFe protein is that certain cysteine thiol groups from the apo-MoFe are susceptible to alkylation whereas the corresponding residues in the mature MoFe protein are not ([*46*], Figure 2). Also, on the basis of AlF_4^--dependent complex formation, and the ΔL127 Fe protein complex formation experiments, interactions between the Fe protein and the apo-MoFe protein do not appear to be as effective as interactions between the Fe protein and the MoFe protein. However, whatever the differences in the folding pattern between the MoFe protein and the apo-MoFe protein, perturbations at the psuedosymmetric $\alpha\beta$-subunit interface are likely to be minimal. This conclusion is based on the observation that Fe protein and apo-MoFe protein are able to interact in a such a way that a high rate of MgATP hydrolysis capability is maintained. In this context it is noted that the three-dimensional model of the MoFe-protein$-$Fe protein complex shows that the Fe protein contacts the MoFe protein at its $\alpha\beta$-subunit interface and in the closest possible proximity to the P cluster (*53, 67, 68*).

Electron Transfer to the Apo-MoFe Protein. Because apo-MoFe protein is able to catalyze a high level of Fe protein-dependent MgATP hydrolysis, and because we were able to elicit the P^{1+} and P^{2+} oxidation states within the apo-MoFe protein, it was of interest to determine if nucleotide-dependent electron transfer from the Fe protein to the apo-MoFe protein could also occur. Figure 8 shows that the oxidized apo-MoFe protein is able to accept an electron from the Fe protein in a MgATP-dependent manner. In these experiments apo-MoFe protein in the P^{2+} state was prepared and mixed with reduced Fe protein and either MgADP or MgATP. In the presence of MgADP the P^{2+} parallel mode $g \approx 11.8$ EPR is apparent (Figure 8A) as is the $S = {}^1/_2$ perpendicular mode EPR signal characteristic of the reduced Fe protein (Figure 8B). However, in the presence of MgATP, the P^{2+} parallel mode signal disappears (Figure 8A), the $S = {}^1/_2$ perpendicular mode EPR signal of the Fe protein also disappears (as it becomes oxidized to the diamagnetic state), and the P^{1+} $S = {}^1/_2$ perpendicular mode signal becomes apparent as the P cluster is reduced from the P^{2+} state to the P^{1+} state.

Relevance of the UV/Vis Spectrum of As-Isolated and Oxidized Apo-MoFe Protein. In the normal nitrogenase reaction, the reduced and MgATP-bound Fe protein complexes with the MoFe protein followed by an intercomponent electron-transfer event that is intimately associated with nucleotide hydrolysis. The rate of oxidation of the Fe protein that occurs during these events can be followed in real time by monitoring the increase in the A_{430} by stopped-flow spectroscopy. Similarly, the rate of dissociation of the component proteins can be measured by the decrease in the A_{430} that occurs when the oxidized Fe protein is released from the complex and becomes reduced. An example of the latter type of experiment is shown in Figure 7. In these experiments it is shown that the Fe protein dissociates from the apo-MoFe protein at a rate that is only modestly faster than the Fe protein-MoFe protein dissociation. By using this type of analysis, Lowe and Thorneley have developed a kinetic model for nitrogenase catalysis and have shown that the rate-limiting step under optimum turnover conditions is the dissociation of the component proteins (*34*). Although stopped-flow determination of the rate constant of primary electron transfer is straightforward, the smaller, kinetically complex absorbance changes that occur after primary electron transfer have not yet been adequately explained. As an example, a small increase in the absorbance at A_{430} that occurs in stopped-flow experiments after about 0.5 s has been proposed to be the result of P cluster oxidation (*69*). Although oxidation of the P clusters might occur at this stage, our finding that the UV/vis spectrum of the apo-MoFe protein does not change upon IDS-oxidization does not support the possibility that any absorbance changes that occur in stopped-flow experiments can be attributed to oxidation of the P cluster to the P^{2+} state. However, the previous investigation (*69*) suggested that the changes in the P cluster A_{430} are most likely arising from the P^{3+} oxidation state (*31, 70*) of the P cluster which was not examined in the present work. Furthermore, the previous studies (*69*) examined EPR

samples flash frozen after ~5 s, whereas the stopped-flow experiments examined time domains of less than one second, so the possibility of a kinetic rearrangement of the P cluster that might give rise to a change in the A_{430} cannot be discounted.

In summary, a method has been developed for the large-scale purification of an apo-MoFe protein that contains intact P clusters and that can be activated by the simple addition of FeMo-cofactor. The availablity of such an apo-MoFe protein can now be used to advance studies aimed at determining the role of P clusters in the nitrogenase catalytic mechanism.

ACKNOWLEDGMENT

The authors thank Jeannine Chan for experimental assistance and for critically reading this manuscript. We also thank Matthew Ryle for critically reading the manuscript.

REFERENCES

1. Tal, S., Chun, T. W., Gavini, N., and Burgess, B. K. (1991) *J. Biol. Chem. 266*, 10654−657.
2. Dean, D. R., Bolin, J. T., and Zheng, L. (1993) *J. Bacteriol. 175*, 6737−6744.
3. Georgiadis, M. M., Komiya, H., Chakrabarti, P., Woo, D., Kornuc, J. J., and Rees, D. C. (1992) *Science 257*, 1653−1659.
4. Kim, J., and Rees, D. C. (1992) *Science 257*, 1677−1682.
5. Burgess, B. K. (1990) *Chem. Rev. 90*, 1377−1406.
6. Peters, W. P., Stowell, M. H. B., Soltis, M. S., Finnegan, M. G., Johnston, M. K., and Rees, D. C. (1997) *Biochemistry 36*, 1181−1197.
7. Seefeldt, L. C., and Dean, D. R. (1997) *Acc. Chem. Res. 30*, 260−266.
8. Surerus, K. K., Hendrich, M. P., Christie, P. D., Rottgardt, D., Orme-Johnson, W. H., and Münck, E. (1992) *J. Am. Chem. Soc. 114*, 8579−8590.
9. Burgess, B. K., Jacobs, D. B., and Stiefel, E. I. (1980) *Biochim. Biophys. Acta 614*, 196−209.
10. Kim, C.-H., Newton, W. E., and Dean, D. R. (1995) *Biochemistry 34*, 2798−2808.
11. Paustian, T. D., Shah, V. K., and P., R. G. (1990) *Biochemistry 29*, 3515−3522.
12. Hawkes, T. R., and Smith, B. E. (1983) *Biochem. J. 209*, 43−50.
13. Brigle, K. E., Newton, W. E., and Dean, D. R. (1985) *Gene 37*, 37−44.
14. Vieira, J., and Messing, J. (1982) *Gene 19*, 259−268.
15. Page, W. J., and von Tigerstrom, M. (1979) *J. Bacteriol. 139*, 1058−1061.
16. Jacobson, M. R., Cash, V. L., Weiss, M. C., Laird, N. F., Newton, W. E., and Dean, D. R. (1989) *Mol. Gen. Genet. 219*, 49−57.
17. Robinson, A. C., Burgess, B. K., and Dean, D. R. (1986) *J. Bacteriol. 166*, 180−186.
18. Joerger, R. D., and Bishop, P. E. (1988) *J. Bacteriol. 170*, 1475−1487.
19. Vieira, J., and Messing, J. (1987) *Methods Enzymol. 153*, 3−11.
20. Strandberg, G. W., and Wilson, P. W. (1968) *Can. J. Microbiol. 14*, 25−31.
21. Scott, D. J., Dean, D. R., and Newton, W. E. (1992) *J. Biol. Chem. 267*, 20002−20010.
22. Shah, V. K., Davis, L. C., and Brill, W. J. (1972) *Biochim. Biophys. Acta 256*, 498−511.
23. Chromy, V., Fischer, J., and Kulhanek, V. (1974) *Clin. Chem. 20*, 1362−1363.
24. Laemmli, U. K. (1970) *Nature 227*, 680−685.
25. Peters, J. W., Fisher, K., and Dean, D. R. (1994) *J. Biol. Chem. 269*, 28076−28083.
26. Shah, V. K., and Brill, W. J. (1977) *Proc. Natl. Acad. Sci. U.S.A. 74*, 3249−53.
27. Ennor, A. H. (1957) *Methods Enzymol. 3*, 850−856.
28. Fortune, W. B., and Mellon, M. G. (1938) *Ind. Eng. Chem. Anal. Ed. 10*, 61−64.
29. Seefeldt, L. C., and Ensign, S. A. (1994) *Anal. Biochem. 221*, 379−386.
30. Ryle, M., and Seefeldt, L. (1996) *Biochemistry 35*, 4766−4775.
31. Pierik, A. J., Wassink, H., Haaker, H., and Hagen, W. R. (1993) *Eur. J. Biochem. 212*, 51−61.
32. Hagen, W. R. (1992) in *Advances in Inorganic Chemistry* (Sykes, A. G., and Cammack, R., Eds.) pp 165−222, Academic Press, New York.
33. Dutton, P. L. (1978) *Methods Enzymol. 54*, 411−35.
34. Thorneley, R. N. F., and Lowe, D. J. (1983) *Biochem. J. 215*, 393−403.
35. Thorneley, R. N. F. (1975) *Biochem. J. 145*, 391−396.
36. Fisher, K., Lowe, D. J., and Thorneley, R. N. F. (1991) *Biochem. J. 279*, 81−85.
37. Lanzilotta, W. N., Fisher, K., and Seefeldt, L. C. (1996) *Biochemistry 35*, 7188−7196.
38. Duyvis, M. G., Wassink, H., and Haaker, H. (1996) *FEBS Lett. 380*, 233−236.
39. Renner, K. A., and Howard, J. B. (1996) *Biochemistry 35*, 5353−5358.
40. Li, J.-G., Tal, S., Robinson, A. C., Dang, V., and Burgess, B. K. (1990) *J. Bacteriol. 172*, 5884−5891.
41. Orme-Johnson, W. H., Hamilton, W. D., Jones, T. L., Tso, M. Y. W., Burris, R. H., Shah, V. K., and Brill, W. J. (1972) *Proc. Natl. Acad. Sci. U.S.A. 69*, 3142−3145.
42. Imam, S., and Eady, R. R. (1980) *FEBS Lett. 110*, 35−38.
43. Jeng, D. Y., Morris, J. A., and Mortenson, L. E. (1970) *J. Biol. Chem. 245*, 2809−2813.
44. Watt, G. D., Bulen, W. A., Burns, A., and Hadfield, K. L. (1975) *Biochemistry 14*, 4266−4272.
45. Deits, T. L., and Howard, J. B. (1990) *J. Biol. Chem. 265*, 3859−3867.
46. Magnuson, J. K., Paustian, T. D., Shah, V. K., Dean, D. R., Roberts, G. P., Rees, D. C., and Howard, J. B. (1997) *Tetrahedron 53*, 11971−11984.
47. Watt, G. D., and Wang, Z.-C. (1989) *Biochemistry 28*, 1844−1850.
48. Watt, G. D., and Wang, Z.-C. (1986) *Biochemistry 25*, 5196−5202.
49. Rawlings, J., Shah, V. K., Chisnell, J. R., Brill, W. J., Zimmerman, R., Münck, E., and Orme-Johnson, W. H. (1978) *J. Biol. Chem. 1978*, 1001−1004.
50. Tittsworth, R. C., and Hales, B. J. (1993) *J. Am. Chem. Soc. 115*, 9763−9767.
51. Lanzilotta, W. N., Christiansen, J., Dean, D. R., and Seefeldt, L. C. (1998) *Biochemistry* (in press).
52. Burgess, B. K., and Lowe, D. J. (1996) *Chem. Rev., 96*.
53. Schindelin, H., Kisker, C., Schlessman, J. L., Howard, J. B., and Rees, D. C. (1997) *Nature 22*, 370−376.
54. Zumft, W. G., Mortenson, L. E., and Palmer, G. (1974) *Eur. J. Biochem. 46*, 525−535.
55. Homer, M. J., Dean, D. R., and Roberts, G. P. (1995) *J. Biol. Chem. 270*, 24745−24752.
56. Kim, J., and Rees, D. C. (1992) *Nature 360*, 553−560.
57. Homer, M. J., Paustian, T. D., Shah, V. K., and Roberts, G. P. (1993) *J. Bacteriol. 175*, 4907−4910.
58. White, T. C., Harris, G. S., and Orme-Johnson, W. H. (1992) *J. Biol. Chem. 267*, 24007−24016.
59. Jacobson, M. R., Brigle, K. E., Bennett, L. T., Setterquist, R. A., Wilson, M. S., Cash, V. L., Beynon, J., Newton, W. E., and Dean, D. R. (1989) *J. Bacteriol. 171*, 1017−1027.
60. Jacobson, M. R., Premakumar, Z., and Bishop, P. E. (1986) *J. Bacteriol. 167*, 480−6.
61. Orme-Johnson, W. H., and Sands, R. H. (1973) in *Iron Sulfur Proteins* (Lovenberg, W., Ed.) pp 195−238, Academic Press, New York.

62. Rupp, H., Rao, K. K., Hall, D. O., and Cammack, R. (1978) *Biochim. Biophys. Acta 537*, 255−269.
63. Blanchard, C. Z., and Hales, B. J. (1996) *Biochemistry 35*, 472−478.
64. Gavini, N., Ma, L., Watt, G. D., and Burgess, B. K. (1994) *Biochemistry 33*, 11842−11849.
65. Zimmerman, R., Münck, E., Brill, W. J., Shah, V. K., Henzl, M. T., Rawlings, J., and Orme-Johnson, W. H. (1978) *Biochim. Biophys. Acta 537*, 185−207.
66. Robinson, A. E., Richards, A. J. M., Thomson, A. J., Hawkes, T. R., and Smith, B. E. (1984) *Biochem. J. 219*, 495−503.
67. Howard, J. B. (1993) in *Molybdenum Enzymes, Cofactors, and Model Systems* (Stiefel, E. I., Coucouvanis, D., and Newton, W. E., Eds.) pp 271−289, American Chemical Society, Washington, DC.
68. Rees, D. C., Schindelin, H., Kisker, C., Schlessman, J., Peters, J. W., Seefeldt, L. C., and Howard, J. B. (1998) in *Biological Nitrogen Fixation for the 21st Century* (Elmerich, C., Kondorosi, A., and Newton, W. E., Eds.) pp 11−16, Kluwer Academic Publishers, Dordrecht, The Netherlands.
69. Lowe, D. J., Fisher, K., and Thorneley, R. N. F. (1993) *Biochem. J. 292*, 93−98.
70. Hagen, W. R., Wassink, H., Eady, R. R., Smith, B. E., and Haaker, H. (1987) *Eur. J. Biochem. 169*, 457−465.

BI981165B